Nanodevices

DOI: 10.1002/ange.201107591

Programmed Dynamic Topologies in DNA Catenanes**

*Johann Elbaz, Zhen-Gang Wang, Fuan Wang, and Itamar Willner**

Topological nanostructures of DNA generated by the condensation or relaxation of nucleic acids biopolymers have important functions in cellular processes.[1] Mechanically interlocked topologies of DNA catenanes were identified in nature,[2] and substantial research efforts were directed towards the synthesis of manmade nucleic acid based catenanes.[3–5] The programmed dynamic reconfiguration of the topologies of DNA catenanes is, however, an unresolved challenge in DNA nanotechnology. Ingenious methods for the synthesis of molecular[6,7] or macromolecular polymeric catenanes[8] have been reported, and the stimuli-controlled reversible reconfiguration of molecular topologies was demonstrated. Triggers, such as electron transfer[9] or optically induced photoisomerization,[10] were used to mechanically reconfigure catenated molecular nanostructures, and the systems acted as reversible switches or molecular motors.[11] Herein, we report on the synthesis of two-ring and three-ring catenated DNA nanostructures, and demonstrate the programmed reconfiguration of the DNA catenanes by using externally added nucleic acids as input stimuli. Specifically, we highlight the directional, dynamic, and reversible reconfiguration of the catenanes through the instructive information introduced by the coadded inputs that result in dictated strand-displacement processes. While in a previous report a programmed transformation of an origami construct into a catenane nanostructure was demonstrated,[4] this process was unidirectional, and transformed one structure into a second topology. In the present system, control of the dynamic directional processes over reversible interconversion across three distinct topologies is demonstrated.

DNA-based nanotechnology is a rapidly developing research field that makes use of the structural and functional information encoded in the base sequence of the nucleic acid strands. This encoded information was extensively implemented to self-assemble two-dimensional[12] and three-dimensional[13–20] DNA nanostructures, to use DNA for computing,[21–23] and for sensing.[24] Particularly interesting is the application of DNA as a functional material for the construction of supramolecular machines.[25,26] Different DNA nanostructures that perform mechanical or motor functions, such as "tweezers"[27] or "walkers",[28] have been reported. The diversity of mechanically interlocked DNA nanostructures, such as catenanes,[3–5] rotaxanes,[29] or borromean rings,[30] paves the way to engineer nanomachines revealing predesigned properties and functions. The present study describes the synthesis of two-ring and three-ring catenated DNA nanostructures (ca. 7 nm diameter) that are structurally characterized, and implemented for dictated nanomechanical processes.

The synthesis of the two-ring DNA catenane is outlined in Figure 1 A. The resulting catenane was purified by denaturing gel electrophoresis (Figure 1 B) and characterized by AFM

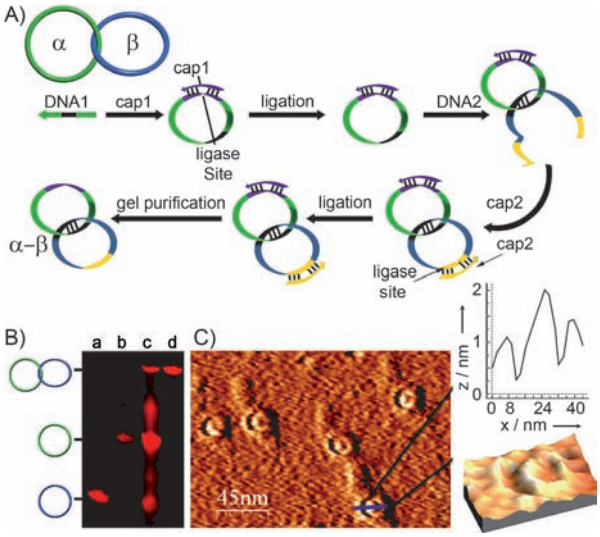

Figure 1. A) Representation of the synthesis of the α–β-catenane system. It involves the capping of a single-stranded nucleic acid (DNA 1), followed by the ligation of the 3′ and 5′ ends to form a circular DNA. The threading of the nucleic acid (DNA 2) through the circle by hybridization of the respective domain (hybridization should be limited to ten bases or less to allow a single helix turn) was followed by the capping of the threaded nucleic acid and ligating of its 3′ and 5′ ends to form, after removal of the caps, the catenane structure consisting of ring α and ring β. B) Denaturing gel electrophoresis results of the α–β-catenane rings, lanes: a) ring β only; b) ring α only; c) after synthesis of the two-ring catenane; d) the two-ring catenane after purification. C) AFM images of the α–β-catenane rings and its appropriate cross-section analysis.

(Figure 1 C). It should be noted that while synthesizing the interlocked catenanes, a duplex, non-interlocked, bicircular structure of ring α and ring β can be formed, yet this structure is eliminated during the purification process under denaturing gel electrophoresis. Thus, the system under investigation is a pure interlocked catenane. Cross-section analysis clearly

[*] J. Elbaz,[+] Dr. Z.-G. Wang,[+] Dr. F. Wang, Prof. I. Willner
Institute of Chemistry
Center of Nanoscience and Nanotechnology
The Hebrew University of Jerusalem
Jerusalem 91904 (Israel)
E-mail: willnea@vms.huji.ac.il

[+] These authors contributed equally to this work.

[**] This study was supported by the Volkswagen Foundation (Germany). J.E. acknowledges a Converging Technologies Fellowship (Israel Science Foundation).

Supporting information for this article is available on the WWW under http://dx.doi.org/10.1002/anie.201107591.

supports the two-ring structure, where the external rails exhibit heights of approximately 1 nm, characteristic of single-stranded DNA, while the central duplex domain of the catenane has a height of approximately 2 nm, consistent with the formation of duplex structure. The reversibly triggered translocation of the two-ring catenane is exemplified in Figure 2. Ring α and ring β are initially interlocked by hybridization in domain I. The hybridization of ring β to domain I is energetically favored relative to domain II (9 base pairs versus 7 base pairs, including one mismatch. For a detailed description of the sequences and the consequences for the dynamic topologies of the rings, see Table S1 and Figure S1 in the Supporting Information, as well as the accompanying discussions).The moving ring β is functionalized with the quencher unit Q through hybridization. Ring α is alternately functionalized with the nucleic acids B_1 or B_2 that are modified with fluorophores F_1 or F_2, respectively (see Table S1 in the Supporting Information). Interaction of the catenane with the fuel DNA (Fu) results in the strand displacement of domain I of ring α, and the translocation of ring β to its second hybridization site, domain II. When ring α is blocked through hybridization to nucleic acid F_1-B_1, ring β translocates through the lower rail to position II (path a). In turn, the blocking of the lower rail with the nucleic acid F_2-B_2 leads to the translocation of ring β to position II through the upper rail of ring α (path b). The subsequent displacement of the Fu by the antifuel strand (AFu), which is fully complementary to Fu, leads to the reverse translocation of the ring β to domain I. The respective fluorescence properties of F_1 and F_2 provide the readout signal for the mechanical topological transformations in the two-ring catenane system. While in the states "C_1" and "C_1*" the fluorophore F_1 is effectively quenched, and fluorophore F_2 exhibits high fluorescence intensity, in states "C_2" and "C_2*" fluorophore F_1 exhibits high fluorescence while fluorophore F_2 is quenched. The insets in Figure 2 show the reversible cyclic fluorescence changes upon activation of the mechanical transformations of the catenated rings by the Fu and AFu strands, using fluorophores F_1 and F_2 as readout labels. It should be noted that upon blocking ring α with both nucleic acids F_1-B_1 and F_2-B_2, the translocation of ring β to domain II was almost fully inhibited (Figure S2 in the Supporting Information). This result suggests that the blocking of ring α with F_1-B_1 results in the directional translocation of ring β to site II and back to site I, through the lower single-stranded rail, whereas the blocking of ring α with F_2-B_2 dictates the translocation of ring β to site II and back to site I through the upper single-stranded rail of ring α (For further support of the directional translocation of the ring, see the discussion of the three-ring catenane system, below.)

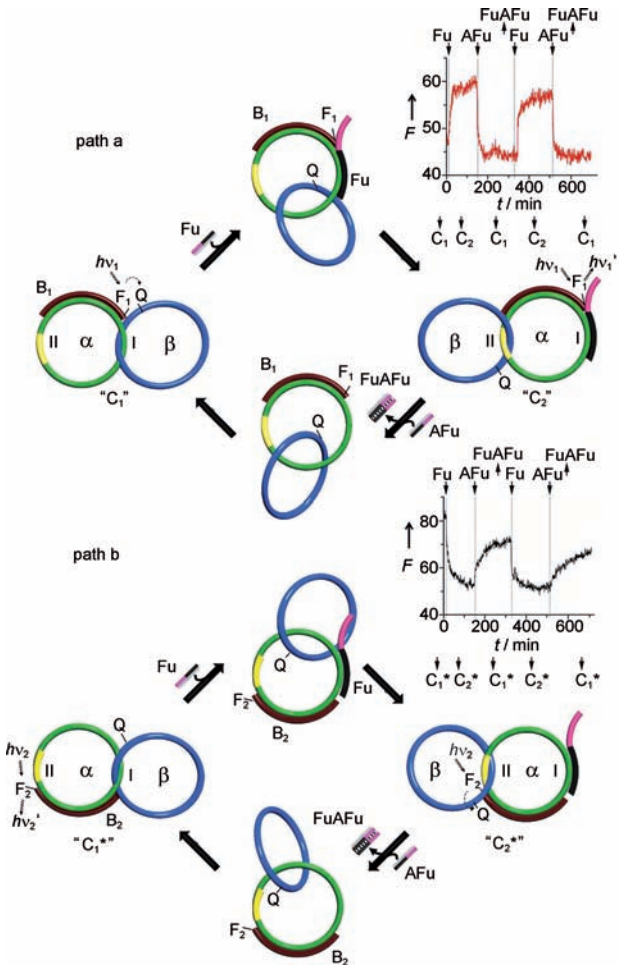

Figure 2. Dynamic translocation pathways of the α–β-catenane system. Path a) The dynamic translocation of ring β between domain I and domain II through the lower rail of ring α, by the addition of Fu and AFu, respectively. Inset: Time-dependent fluorescence changes of F_1 upon the translocation of ring β through the lower rail of ring α. The arrows on top indicate the time of application of the respective DNA Fu and AFu strands resulting in the different topologies C_2 and C_1, respectively. Path b) The dynamic translocation of ring β between domain I and domain II through the upper rail of ring α, by the addition of Fu and AFu, respectively. Inset: Time-dependent fluorescence changes of F_2 upon the translocation of ring β through the upper rail of ring α. The arrows on top indicate the time of application of the respective DNA Fu and AFu strands resulting in the different topologies, C_2* and C_1*, respectively.

The study was then extended by preparing two different three-ring catenated nanostructures, $\alpha_1\beta\gamma$ and $\alpha_2\beta\gamma$ (Figure 3 A), that enabled the controlled, directional, mechanical translocation of one of the rings (see Table S2 and Figure S3 in the Supporting Information for sequences. The synthesis of the three-ring catenane is described in Figure S4 in the Supporting Information). The purity of the three-ring catenane structure $\alpha_1\beta\gamma$ was confirmed by electrophoresis experiments (Figure 3 B; for the denaturing gel electrophoresis of the three catenated rings $\alpha_2\beta\gamma$, see Figure S5 in the Supporting Information), and by AFM measurements that demonstrated, at a single-molecule level, the interlocked structure of the three-ring catenane (Figure 3 C). The cross-section analysis of the "linear" three-ring catenane reveals heights of approximately 1 nm for the single-stranded DNA domains at the edge, and heights of approximately 2 nm for the interlocked duplex regions. Interestingly, while previous double-stranded catenane structures revealed rigid structures in the AFM images,[5] the single-stranded domains in the catenane studied here introduce flexibilities in the nanostructures that are reflected in the AFM images. (For additional AFM images of the catenanes, see Figure S6 in

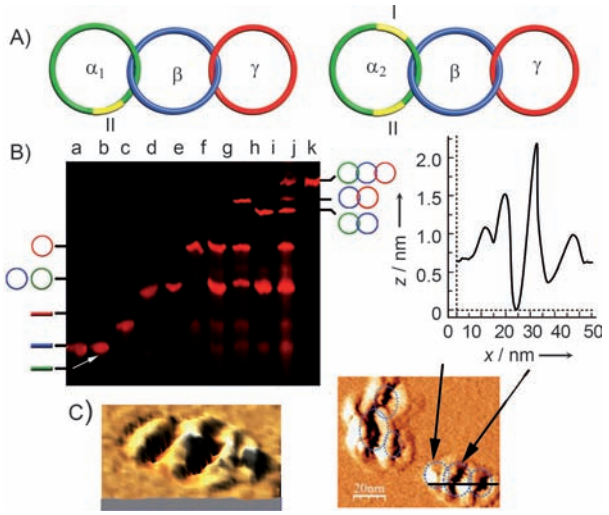

Figure 3. A) Representation of the two different three-ring catenanes, where $\alpha_1\beta\gamma$ includes a single translocation domain of ring γ to ring α_1 (domain II marked in yellow), and $\alpha_2\beta\gamma$ includes two isoenergetic domains for the mechanical moving of ring γ (domain I and domain II marked in yellow). B) Denaturing gel electrophoresis results confirming the purity of the three-ring catenanes. Lanes: a) single-strand DNA prior to the synthesis of ring β; b) single-strand DNA prior to the synthesis of ring α_1; c) single-strand DNA prior to the synthesis of ring γ; d) ring β only; e) Ring α_1 only; f) Ring γ only; g) after the synthetic process that includes only rings α_1 and γ (without the addition of ring β during the synthesis), resulting in two separate rings; h) after the synthetic process that includes only ring β and γ (without the addition of ring α_1 during the synthesis), resulting in the catenated two-ring $\beta\gamma$; i) after the synthetic process that included only ring β and α_1 (without the addition of ring γ during the synthesis), resulting in the $\alpha_1\beta$ catenane rings; j) after the synthetic process that includes all the appropriate nucleic acid strands (ring α_1, ring β, and ring γ), resulting in the three-ring catenanes $\alpha_1\beta\gamma$; k) the pure three-ring catenanes $\alpha_1\beta\gamma$ after the purification process. C) AFM images of the three-ring catenanes, $\alpha_1\beta\gamma$, and the respective cross-section analysis.

the Supporting Information.) In catenane $\alpha_1\beta\gamma$, the ring α_1 includes one hybridization site for the mechanically moving ring γ (domain colored in yellow), whereas catenane $\alpha_2\beta\gamma$ includes two isoenergetic domains for the formation of the respective duplexes with the moving ring γ. (For the detailed analysis of the mechanical translocation of ring γ to the single binding site on ring α_1, see Figure S7 in the Supporting Information.) The mechanical motion of ring γ to ring α_2, which includes the two binding domains I and II, is shown in Figure 4 A. To follow the mechanical motion, rings α_2 and γ were labeled through hybridization with the respective nucleic acid functionalized fluorophore–quencher pairs F_1–Q_1 and F_2–Q_2. In the linear configuration of the three catenated rings "L", the fluorophores and quenchers are apart, leading to high fluorescence intensities. The mechanical compression of the three rings into configurations P_1 or P_2, upon the addition of the Fu, leads to the identical quenching probability of the fluorophores F_1 and F_2, path a. Upon the formation of the compressed configurations P_1 and P_2, the fluorophores F_1 and F_2 are quenched, whereas upon the addition of the AFu strand, the original fluorescence of the "linear" three-ring configuration is restored. The major challenge is, however, the control over the direction of the topological translocation of ring γ to either domain I or domain II associated with ring α_2. This programmed translocation of ring γ was demonstrated by the introduction of specific blocker units, B_1 or B_2, that associate through hybridization and duplex formation with specific domains associated with ring β, path b and path c. Blocking of the upper rim of ring β in the linear configuration "L_1" with B_1 and treatment of the nanostructure with the Fu strand lead to the programmed and selective translocation of ring γ to domain II of ring α_2, configuration P_3, which is imaged by the effective quenching of fluorophore F_2 and inefficient quenching of F_1, path b. Upon treatment of the compressed nanostructure with the AFu strand and the antiblocker strand, AB, the linear three-ring configuration is regenerated. Similarly, the blocking of the lower rim of ring β with the blocker, B_2, and treatment of the resulting nanostructure with the Fu strand, path c, results in the mechanical motion of ring γ through the upper free rail to form the stable, compressed configuration, P_4. The formation of this configuration is confirmed by the effective quenching of F_1 and inefficient quenching of F_2. By treatment of the compressed configuration with the AFu strand and the antiblocker strand, the initial "linear" configuration "L", exhibiting its characteristic fluorescence features, is restored. By the cyclic interaction of configuration "L" with the respective blocker/antiblocker and Fu/AFu strands, the system is fully controlled to undergo the cyclic programmed reconfiguration. Figure 4 B depicts the cyclic and reversible time-dependent fluorescence changes upon blocking the upper or lower rims of ring β separately, and the transition of the three-ring catenanes through the different states. As the fluorescence intensities of F_1 and F_2 in the different topologies are known we elucidated the efficiency of the translocation of ring γ to ring α_2 by the appropriate Fu strands (for detailed explanations, see Figure S8 in the Supporting Information). Accordingly, the experimental fluorescence changes shown in Figure 4 B translate to approximately (85 ± 2) % of the population of ring γ to site I or site II, and to (92 ± 4) % of the regenerated linear configuration, L_1 or L_2. The rate constants for the translocation of ring γ to site I or site II are approximately $k = 0.071\ \text{min}^{-1}$ ($\tau/2 = 14$ min). On the other hand, diffusional transition of a non-interlocked ring exhibits a rate constant of approximately $k = 0.022\ \text{min}^{-1}$ ($\tau/2 = 44$ min). It should be noted that control experiments confirm that the fluorescence changes do not originate from local environmental changes occurring in the nanostructures upon the addition of the DNA strands (see Figure S9 in the Supporting Information).

The blocker strands associated with the two-ring or three-ring catenanes play an essential role in the directional reconfiguration of the catenated topologies. The barrier introduced for the reconfiguration of the ring through the "blocked" domain, may be attributed to steric and/or electrostatic repulsive interactions between the blocked domains and the moving ring. An attempt to elucidate the blocking mechanism was made by constructing a set of three-ring catenanes, where ring β with the two blocking domains was kept constant in size (76 bases), while the reconfigured ring γ was systematically enlarged to include 90, 107, 120, and

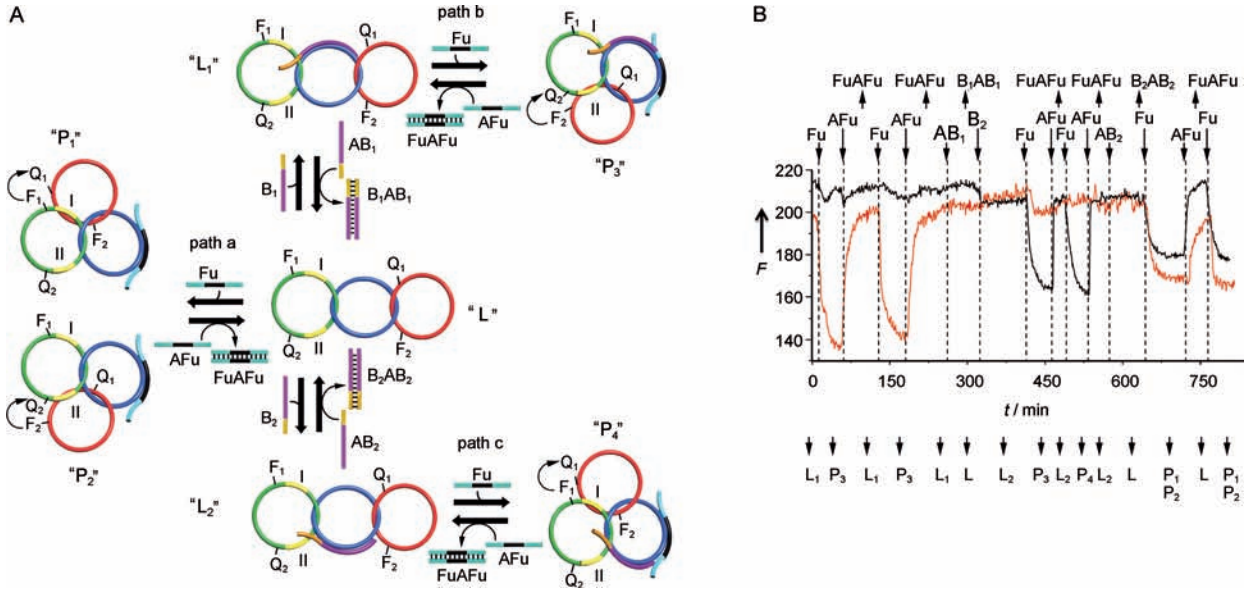

Figure 4. A) Representation of the dynamic programmed translocation of ring γ to domain I and domain II, upon the addition of the respective DNA strands. B) Time-dependent fluorescence changes upon the programmed translocation of ring γ through the upper or lower rail of ring β, leading to the respective topologies "L", "L_1", "L_2", "P_1", "P_2", "P_3", and "P_4". The arrows on top indicate the time of application of the respective DNA strands that results in the different topologies. F_1 = black; F_2 = red.

140 bases. We find that the reconfiguration of ring γ is totally blocked in the set of all nanoengineered catenanes upon the blocking of the two domains on ring β. The selective removal of any of these strands resulted in, as expected, the directional reconfiguration of the catenanes. The lack of sensitivity of the reconfiguration of the nanostructures to the size of ring γ suggests that the blocking effect is not due to a steric effect, but rather originates from electrostatic repulsions. The duplexes associated with the blocking domains yield local electrical fields that repel the conformationally flexible single-stranded ring γ, thus preventing their topological reconfiguration. Moreover, one may argue that the protruding single strand associated with the blocker unit may participate in controlling the barrier for reconfiguration of the ring through the blocked domain. The single strand "tail" does not play, however, any significant role in preventing the translocation of ring γ through the blocked region, and a blocker lacking the protruding tail reveals a similar blocking effect (see Figure S10 in the Supporting Information).

In conclusion, the present study has demonstrated the programmed, directional reconfiguration of DNA catanane topologies (while topology is a major area of mathematics concerned with the properties of objects that are preserved under continuous deformation,[31] the concept of topology was adapted by chemists to describe different stereochemical properties. For the present discussion, topological configurations are considered as constitutional isomers that differ in their bond connectivity.[32] For a detailed discussion on the topologies of catenanes and interlocked DNA structures, see Refs. [32]–[34]). This study made use of the strand-displacement process as the driving mechanism for the topological transitions. Nonetheless, other external stimuli, such as pH or metal ions, may be similarly adapted to induce the topological reconfiguration of the catenanes. The reconfiguration of the catenanes holds promise for multiplex analysis of DNA targets, as two different analytes may be used to displace the two blocker units selectively. It should be noted that the catenated nanostructures include a single-stranded DNA skeleton. This enables the tethering of cargoes, for example, nanoparticles, to the catenane devices and the programmed arrangement of the objects by the motion of the catenanes. Also, these cargoes can be easily exchanged, for example, by using the strand-displacement process. This perspective demonstrates the advantages of the present systems over interlocked molecular catenanes,[7,8] where the translocation of a cargo requires special synthetic efforts, and the exchange of the cargo in the resulting catenane is impossible. Furthermore, the fact that the DNA catenanes that include interlocked cycles are stabilized against hydrolytic digestion may enable the use of these structures as labels in intracellular environments.

Received: October 27, 2011
Revised: December 6, 2011
Published online: January 27, 2012

Keywords: catenanes · DNA structures · molecular devices · nanostructures · strand displacement

[1] A. D. Bates, A. Maxwell, *DNA Topology*, 2nd ed., Oxford University Press, New York, **2005**.
[2] B. Hudson, J. Vinograd, *Nature* **1967**, *216*, 647–652.
[3] Y. Liu, A. Kuzuya, R. Sha, J. Guillaume, R. Wang, J. W. Canary, N. C. Seeman, *J. Am. Chem. Soc.* **2008**, *130*, 10882–10883.
[4] D. Han, S. Pal, Y. Liu, H. Yan, *Nat. Nanotechnol.* **2010**, *5*, 712–717.
[5] T. L. Schmidt, A. Heckel, *Nano Lett.* **2011**, *11*, 1739–1742.

[6] C. O. Dietrich-Buchecker, J. P. Sauvage, J. P. Kitzinger, *Tetrahedron Lett.* **1983**, *24*, 5095 – 5098.
[7] D. B. Amabilino, P. R. Ashton, M. S. Tolley, J. F. Stoddart, D. J. Williams, *Angew. Chem.* **1993**, *105*, 1358 – 1362; *Angew. Chem. Int. Ed. Engl.* **1993**, *32*, 1297 – 1301.
[8] J. M. Spruell, A. Coskun, D. C. Friedman, R. S. Forgan, A. A. Sarjeant, A. Trabolsi, A. C. Fahrenbach, G. Barin, W. F. Paxton, S. K. Dey, M. A. Olson, D. Benítez, E. Tkatchouk, M. T. Colvin, R. Carmielli, S. T. Caldwell, G. M. Rosair, S. G. Hewage, F. Duclairoir, J. L. Seymour, A. M. Z. Slawin, W. A. Goddard III, M. R. Wasielewski, G. Cooke, J. F. Stoddart, *Nat. Chem.* **2010**, *2*, 870 – 879.
[9] C. P. Collier, G. Mattersteig, E. W. Wong, Y. Luo, K. Beverly, J. Sampaio, F. M. Raymo, J. F. Stoddart, J. R. Heath, *Science* **2000**, *289*, 1172 – 1175.
[10] V. Balzani, A. Credi, M. Venturi, *Chem. Soc. Rev.* **2009**, *38*, 1542 – 1550.
[11] E. R. Kay, D. A. Leigh, F. Zerbetto, *Angew. Chem.* **2007**, *119*, 72 – 196; *Angew. Chem. Int. Ed.* **2007**, *46*, 72 – 191.
[12] E. Winfree, L. Furong, L. A. Wenzler, N. C. Seeman, *Nature* **1998**, *394*, 539 – 544.
[13] H. Yan, S. H. Park, G. Finkelstein, J. H. Reif, T. H. LaBean, *Science* **2003**, *301*, 1882 – 1884.
[14] F. A. Aldaye, A. Palmer, H. F. Sleiman, *Science* **2008**, *321*, 1795 – 1799.
[15] J. Chen, N. C. Seeman, *Nature* **1991**, *350*, 631 – 633.
[16] P. Goodman, I. A. T. Schaap, C. F. Tardin, C. M. Erben, R. M. Berry, C. F. Schmidt, A. J. Turberfield, *Science* **2005**, *310*, 1661 – 1665.
[17] Y. He, T. Ye, M. Su, C. Zhang, A. E. Ribbe, W. Jiang, C. Mao, *Nature* **2008**, *452*, 198 – 201.
[18] E. S. Andersen, M. Dong, M. M. Nielsen, K. Jahn, R. Subramani, W. Mamdouh, M. M. Golas, B. Sander, H. Stark, C. L. P. Oliveira, J. S. Pedersen, V. Birkedal, F. Besenbacher, K. V. Gothelf, J. Kjems, *Nature* **2009**, *459*, 73 – 76.
[19] H. Dietz, S. M. Douglas, W. M. Shih, *Science* **2009**, *325*, 725 – 730.
[20] P. W. K. Rothemund, *Nature* **2006**, *440*, 297 – 302.
[21] G. Seelig, D. Soloveichik, D. Y. Zhang, E. Winfree, *Science* **2006**, *314*, 1585 – 1589.
[22] J. Elbaz, O. Lioubashevski, F. Wang, F. Remacle, R. D. Levine, I. Willner, *Nat. Nanotechnol.* **2010**, *5*, 417 – 422.
[23] Z. G. Wang, J. Elbaz, F. Remacle, R. D. Levine, I. Willner, *Proc. Natl. Acad. Sci. USA* **2011**, *107*, 21996 – 22001.
[24] F. Wang, J. Elbaz, C. Teller, I. Willner, *Angew. Chem.* **2011**, *123*, 309 – 313; *Angew. Chem. Int. Ed.* **2011**, *50*, 295 – 299.
[25] J. Bath, A. J. Turberfield, *Nat. Nanotechnol.* **2007**, *2*, 275 – 284.
[26] Y. Krishnan, F. C. Simmel, *Angew. Chem.* **2011**, *123*, 3180 – 3215; *Angew. Chem. Int. Ed.* **2011**, *50*, 3124 – 3156.
[27] B. Yurke, A. J. Turberfield, A. P. Mills, F. C. Simmel, J. L. Neumann, *Nature* **2000**, *406*, 605 – 608.
[28] Y. S. Shin, N. A. Pierce, *J. Am. Chem. Soc.* **2004**, *126*, 10834 – 10835.
[29] D. Ackermann, T. L. Schmidt, J. S. Hannam, C. S. Purohit, A. Heckel, M. Famulok, *Nat. Nanotechnol.* **2010**, *5*, 436 – 442.
[30] C. Mao, W. Sun, N. C. Seeman, *Nature* **1997**, *386*, 137 – 138.
[31] W. Basener, *Topology and Its Applications*, Wiley, Hoboken, NJ, **2006**.
[32] D. M. Walba, *Tetrahedron* **1985**, *41*, 3161 – 3212.
[33] G. Schill, *Catenanes, Rotaxanes and Knots*, Academic Press, New York, **1971**.
[34] J. Vinograd, J. Lebowitz, R. Radloff, R. Watson, P. Laipis, *Biochemistry* **1965**, *53*, 1104.

